Carbon 173 (2021) 901–909

Contents lists available at ScienceDirect

Carbon

journal homepage: www.elsevier.com/locate/carbon

Research Article

Deep-injection floating-catalyst chemical vapor deposition to continuously synthesize carbon nanotubes with high aspect ratio and high crystallinity

Sung-Hyun Lee [a, 1], Junbeom Park [a, 1], Ji Hong Park [a, b, 1], Dong-Myeong Lee [a, c, 1], Anna Lee [d], Sook Young Moon [a], Sei Young Lee [e, **], Hyeon Su Jeong [a, ***], Seung Min Kim [a, *]

[a] Institute of Advanced Composite Materials, Korea Institute of Science and Technology (KIST), Jeonbuk, 55324, Republic of Korea
[b] Department of Materials Science and Engineering, Korea Advanced Institute of Science and Technology (KAIST), Daejeon, 34141, Republic of Korea
[c] Department of Chemical and Biomolecular Engineering, Korea Advanced Institute of Science and Technology (KAIST), Daejeon, 34141, Republic of Korea
[d] Department of Chemistry, Jeonbuk National University, Jeonju, 54896, Republic of Korea
[e] Department of Biomedical Engineering, Yonsei University, Kangwon, 26493, Republic of Korea

ARTICLE INFO

Article history:
Received 7 September 2020
Received in revised form
18 November 2020
Accepted 22 November 2020
Available online 27 November 2020

Keywords:
Carbon nanotube
High-aspect ratio
High-crystallinity
Carbon nanotube fiber
High-strength

ABSTRACT

The deep-injection floating-catalyst chemical vapor deposition (DI-FCCVD) technique is introduced to continuously synthesize carbon nanotubes (CNTs) with high aspect ratio (AR>17000) and high crystallinity (I_G/I_D > 60) at high production rate (>6 mg/min). In this technique all reactants are injected directly and rapidly into high-temperature reaction zone through thin alumina tube; this process leads to simultaneous thermal decomposition of well-mixed catalyst precursors (ferrocene and thiophene), and thus to formation of uniformly-sized catalyst particles. Carbon nanotube fiber (CNTF) fabricated from high-AR CNT has specific strength of 2.94 N/tex and specific modulus of 231 N/tex, which are comparable to those of the state-of-the-art carbon fiber. Both DI-FCCVD and wet spinning methods are easily scalable to mass production, so this study may enable widespread industrial application of CNTFs.

1. Introduction

A carbon nanotube (CNT) is a giant one-dimensional molecule composed of nearly-perfect sp^2-bonded carbon atoms. Highly-crystalline CNTs have few defects and therefore have exceptional mechanical, electrical, and thermal properties [1–5]. However, the potential of CNTs has not been yet fully exploited in industry because the properties of CNT-based macrostructures are dominated by contacts among tubes rather than by the number of defects with them. Therefore, to improve the properties of CNT macrostructures, the number density of inter-tube contacts must be reduced. For this purpose, the aspect ratios (ARs) of CNTs must be increased. CNTs with extremely high AR would minimize the number of contacts between tubes in CNT macrostructures, so their properties could be maximized and might approach those of CNTs.

CNT fibers (CNTFs) are the CNT macrostructures to which the intrinsic properties of CNTs can be best transferred due to their mutual dimensional consistency. High-performance CNTFs can be obtained by wet spinning of a liquid crystal (LC) phase of CNT and chlorosulfonic acid (CSA) solution without surfactant [6–11]. To form the LC phase, CNTs must be highly crystalline with high AR [12,13]. The properties of CNTFs increase linearly as ARs of constituent CNTs increase [6]. Therefore, synthesis of high-performance CNTFs requires CNTs that have both high AR and high crystallinity. Additionally, practical applications of CNTs requires synthesis at reasonably high rates.

Scalable synthesis of CNTs that have both high AR and high crystallinity has not been yet accomplished and is considered to be very difficult task. So far, the highest AR of CNT from which CNTFs

* Corresponding author.
** Corresponding author.
*** Corresponding author.
E-mail addresses: syl235@yonsei.ac.kr (S.Y. Lee), jeonghs98@kist.re.kr (H.S. Jeong), seungmin.kim@kist.re.kr (S.M. Kim).
[1] These authors contributed equally to this work.

https://doi.org/10.1016/j.carbon.2020.11.065
0008-6223/

have been successfully fabricated by the wet spinning is 6700; the CNTF had a specific strength reaching 2.1 N/tex [11]. The study also reported that CNTs with the AR = 9610 were dispersed in CSA but the amount was insufficient to be spun into a fiber [6]. CNTs with the long lengths (~1.5 mm) estimated from the transmission electron microscopy (TEM) images were continuously synthesized by a floating-catalyst chemical vapor deposition (FCCVD) method [14], but these CNTs were not tested for the wet spinning.

CNTs grow from metallic catalyst particles with a few nanometer sizes during a CVD process. Intuitively, to synthesize CNTs with high AR, the size distribution of catalyst particles should be well maintained during CNT synthesis [15,16]. To do so, the synthesis temperatures should be lowered to minimize thermally-activated coarsening of catalyst particles. However, synthesis of highly-crystalline CNTs usually requires high temperature. Thus, simultaneous fulfilment of both requirements is a difficult task; the need for relatively high productivity complicates it further.

This work introduces deep-injection FCCVD (DI-FCCVD), which is a technique to continuously synthesize highly-crystalline CNTs (I_G/I_D > 60) with the highest AR (>17000) reported so far, at a relatively high production rate (>6 mg/min). In this technique, a thin alumina (Al_2O_3) injection tube (inner diameter: 4 mm) is inserted deeply into the high-temperature zone of the reactor. The synthesized CNT can be spun into high-strength CNTF (2.94 N/tex), which is the strongest so far among wet-spun CNTFs. To the best of our knowledge, this is the first demonstration from the synthesis of highly-crystalline spinnable CNTs with high AR to the scalable fabrication of high-strength CNTFs.

2. Experimental Section

2.1. Synthesis of CNTs

CNTs were continuously synthesized by FCCVD using a horizontal reactor. The reactor consists of an electric furnace and an alumina tube that has an inner diameter of 5 cm and a length of 120 cm. Methane (CH_4) was used as the carbon precursor, ferrocene ($C_{10}H_{10}Fe$) as the catalyst precursor, and thiophene (C_4H_4S) as the promoter. Ferrocene and thiophene were purchased from Sigma Aldrich (South Korea) and used without further purification. Argon (Ar) (99.999%) and hydrogen (H_2) (99.999%) were used as the carrier gas. Argon, hydrogen, methane, ferrocene and thiophene are injected together into the reactor through an alumina injection tube (inner diameter: 4 mm). Overall flow rate of methane, hydrogen and argon was 3200 sccm and the synthesis temperature was set at 1200 °C. Ferrocene was held in a chamber that was maintained at 60 °C and thiophene was held in a chamber that was maintained at −5 °C. The vapor pressures of ferrocene and thiophene are determined by the relationship between temperature and vapor pressure [17,18]. The amounts of ferrocene and thiophene were controlled by the flow rates of argon passing through each chamber and calculated using Dalton's law of partial pressure [19]. Detailed synthesis conditions can be found in the Supporting Information (Table S1). The synthesized CNTs were carried to the end of the reactor by the carrier gas, where they were collected on the surface of a rotating rod. Since CNT filaments and aerogels are usually very sticky, they are collected very easily to any rotating rod. In this study, we used the stainless steel rod without any surface treatment. The temperature at the collection position (80−300 °C) is very low compared to the reaction zone (1200 °C). The inner diameter of the alumina injection tube was 4 mm and the depths of the injection tube used in the experiments were 1, 16, 20, 24, 27, 30, or 33 cm from the inlet flange of the reactor. The schematic of the DI-FCCVD method is depicted in Fig. S1.

2.2. Preparation of CNT LC and fabrication of CNTFs

Synthesized CNTs were purified with the following steps: 1) heat-treatment in air at 400 °C for 1 h and 2) immersion in hydrochloric acid (HCl) at 80 °C for 4 h. In this process, the heat-treatment in air at 400 °C for 1 h leads to the removal of the amorphous carbon or carbon shell surrounding iron catalyst particles and the immersion in HCl at 80 °C for 4 h results in the dissolution of iron catalyst particles. Then, purified CNTs were dispersed in CSA. The CNT/CSA solution was blended using a speed mixer (ARE-310 Planetary centrifugal mixer, Thinky) at 2000 rpm for 10 min, and then stirred at 500 rpm for 3 days. The concentrations for finding the transition point from isotropic phase to bi-phase of CNT solutions, which were synthesized at # 4, # 5, and # 6 injection positions were increased from 0.03 mg/mL to 0.14 mg/mL in increments of 0.01 mg/mL. The concentration of CNT and CSA solution for the wet spinning was 5 mg/mL. Briefly, the CNT LC dope was put into a glass syringe and ejected into an acetone coagulation bath at an injection rate of 0.1 mL/min using a 25G needle. The extruded CNTFs were continuously collected on bobbin at winding rate of 5.5 m/min. The collected CNTFs were washed using acetone and distilled water, then dried overnight at 170 °C in a vacuum oven. In some cases, the CNTFs were heated for 30 min at 600 °C in argon (1000 sccm) and hydrogen (500 sccm) atmosphere to completely remove residual CSA.

2.3. Fluid dynamics simulation

To understand the detailed thermal/fluidic characteristics in the FCCVD reactor, we used computational fluid dynamics modeling to solve the continuity, momentum and energy equation in the reactor. Numerical simulation was conducted using Comsol Multiphysics V5.3a (COMSOL, Inc.). The continuity, momentum and energy equations were

$$\nabla \cdot (\rho \boldsymbol{u}) = 0$$

$$\nabla \cdot (\boldsymbol{u} \cdot \nabla)\boldsymbol{u} = \nabla \cdot \left[-p\boldsymbol{I} + \mu\left(\nabla \boldsymbol{u} + (\nabla \boldsymbol{u})^T\right) - \frac{2}{3}\mu(\nabla \cdot \boldsymbol{u})\mathrm{I}\right] + \boldsymbol{F_g}$$

$$\rho C_P \nabla \boldsymbol{u} \cdot \nabla T = \nabla \cdot (k \nabla T) + W_p$$

where ρ [g/cm^3] is the density of the gas, $\boldsymbol{u}$ [m/s] is the velocity field of the gas, p [kg/(m·s^2)] is the fluid pressure, μ [g/(m·s)] is the viscosity of the gas, C_P [J/K, kg·m^2/(s^2·K)] is the thermal capacity of the gas, k [W/(m·K), kg·m/(s^3·K)] is the thermal conductivity of the gas, T [K] is the gas temperature, $\boldsymbol{F_g}$ [m/s^2] is the external force (in this case gravity) and W_p [J, kg·m^2/(s^2)] is the pressure work induced by the density variation**.** The low-Mach-number formulation embedded in Comsol Multiphysics is used to account for density variations. The system has small Reynolds number (<100 based on chamber diameter at 400 °C), so steady-state non-isothermal laminar flow was assumed.

Radiative heat transfer in the reactor and on the injection tube surface was considered, and the shape factor was determined using 'Hemicube' embedded in Comsol. Detailed boundary conditions and coordinate system for numerical simulation are depicted in Fig. S2. The thermal boundary condition for FCCVD reactor was determined from the experimental condition, and the effect of alumina tube on temperature variation of the injection gas was also considered. The mixture of H_2 and Ar in the gas-flow calculation was the same ($[H_2]/[Ar] = 0.64$) as in the CNT synthesis experiment. To verify the simulation model, the numerical results were compared to the temperature distribution without flowing gases in

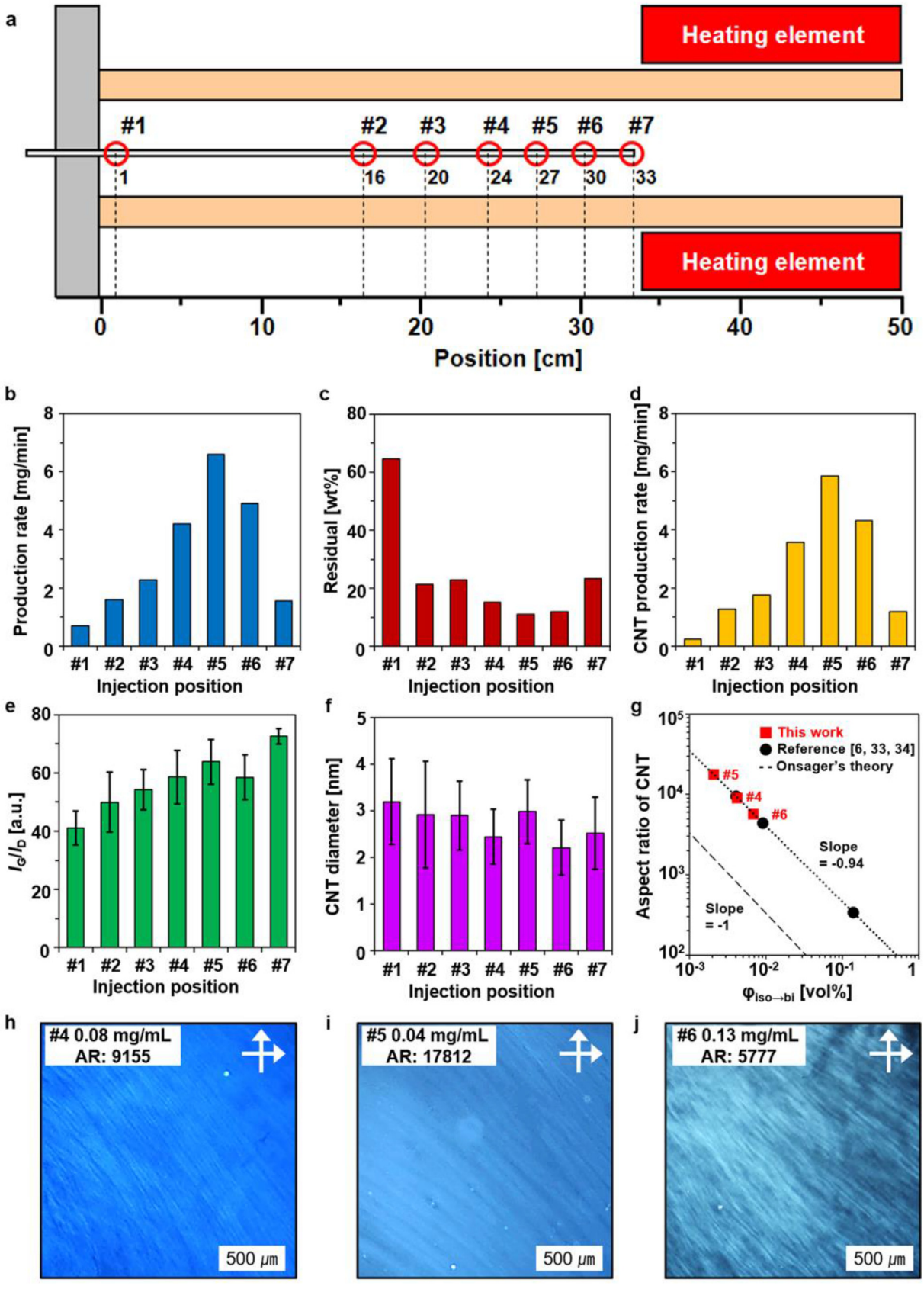

Fig. 1. Synthesis of CNTs by DI-FCCVD. (a) The positions of the injection tube in the horizontal reactor (#1 to #7 correspond to 1 cm, 16 cm, 20 cm, 24 cm, 27 cm, 30 cm, and 33 cm from the inlet flange of the reactor). (b) Production rate, (c) amount of residual catalysts, and (d) CNT production rate of developed DI-FCCVD technique at different positions (insertion depths of thin alumina injection tube). (e) I_G/I_D and (f) diameter of synthesized CNTs depending on the depths of the injection tube. (g) Plots showing Onsager theory and the correlation between the ARs of CNTs and volumetric concentrations ($\phi_{iso\rightarrow bi}$) at which the phase transition from isotropic to bi-phase occurs. This correlation was developed

the reactor with all heaters. Even though the centerline temperature at the inlet shows a little difference, due to complex secondary flow patterns generated by natural convection, overall increase pattern of temperature distribution to the hot zone indicates that this model simulates the thermal flow inside the reactor appropriately.

2.4. In-situ TEM experiment

Iron (Fe)/sulfur (S) catalyst particles were prepared as follow; 1) Ferrocene and sulfur powders were dissolved at 1:1 M ratio in acetone. 2) The solution was sprayed on an E-chip (Protochips), which is a thin membrane device for *in-situ* heating experiment in TEM (Tecnai F20, Thermofisher). 3) The solution-sprayed E-chip was dried to remove acetone to leave only ferrocene and sulfur powders. 4) The dried E-chip was assembled with Fusion (Protochips, *in-situ* TEM holder) and heat-treated at 600 °C for 10 s in a vacuum station (heating rate: 1000 °C/s). 5) Iron particles with sulfur formed on the E-chip during the heat treatment. Iron particles were prepared by the same procedure except for the addition of sulfur powder. The E-chip with grown particles was assembled with Fusion and loaded into the TEM. The appropriate area in which to observe the coarsening and coalescence behaviors of particles was searched at ×450,000 magnification. The atomic ratio (Fe/S) of each particle in observing area was obtained using an energy dispersive X-ray spectroscope (EDS) attached to TEM. The evolutions of particles were captured every 1 min during heating from 500 °C to 800 °C (held for 5 min at each 50 °C step).

2.5. Characterization of CNTs and CNTFs

The production rate was calculated as the weight of product as measured using a digital balance (Mattler Toledo, CP-42) divided by the process time. The residual was obtained by thermogravitic analysis (TGA, Q50, TA Instrument) in air. The crystallinity of CNT was quantified using a Raman spectroscope (Invia, Renishaw) with a 514 nm laser. The diameters and numbers of walls of CNTs were directly measured from the images obtained using TEM. The synthesized CNTs were dispersed in ethanol at a low concentration and the solution was sonicated for the sufficient time (24 h). Afterwards, only CNTs which were isolated or not heavily bundled were analyzed to measure the diameters of CNTs by TEM. The sizes of catalyst particles were measured using ImageJ software from the TEM images. The atomic ratios (Fe/S) of catalyst particles in the CNT sample synthesized at the position #1 were obtained using EDS attached to TEM. The state of dispersion and LC phase of CNT/CSA solution were observed using a polarized optical microscope (POM, LV-100POL, Nikon). The specific strength and modulus of CNTF were measured using a universal testing machine (Favimat+, Textechno) at a tensioning rate of 2 mm/min with the gauge length of 20 mm. The linear density of CNTF was measured by the vibroscopic method using the same universal testing machine. The cross-sectional morphology of CNTF was observed after cutting the CNTF using a focused ion beam - a scanning electron microscopy (FIB-SEM, Scios, Thermofisher). The cross-sectional morphology of CNTF was also observed using TEM after sampling and then thinning the CNTF using FIB-SEM.

3. Results and discussion

FCCVD for CNT synthesis delivers catalyst precursors (ferrocene and thiophene) continuously in the vapor phase into the reactor along with carbon precursor such as methane and carrier gases such as hydrogen and argon. Compared to supported-catalyst CVD method, one of the most distinctive characteristics of FCCVD is the addition of sulfur released from thiophene [20–22]. The ratio of ferrocene to thiophene is a critical factor to determine the crystallinity and productivity of CNTs by FCCVD. Generally, an increase in ferrocene to thiophene ratio increases the crystallinity but decreases the productivity [19,23–25]. Therefore, to synthesize highly-crystalline CNTs at high rates, our DI-FCCVD strategy is to rapidly inject all reactants together into the high-temperature zone of the reactor through a thin tube with relatively high ferrocene to thiophene ratio and high overall gas-flow rate.

The synthesis of CNTs were performed depending on the different depths of the injection tube (Fig. 1). In this study, all synthesis experiments used exactly the same conditions and composition of reactants (ferrocene, thiophene, methane, hydrogen, and argon) except for the depth of injection tube (Experimental Section and Table S1). The molecular ratio of ferrocene to thiophene was set to be 1.6 (mol/mol), which is higher than in most of FCCVD based studies [23,26–28]. Injection position #1 was at the flange of the horizontal reactor (1 cm and 93 °C) (Fig. 1a and Fig. S3); position #7 was farthest from the flange and closest to the hot zone (33 cm and 1046 °C) (Fig. 1a and Fig. S3). The temperatures at the positions of the injection tube were measured without flowing gases but the temperatures were also measured at the positions which is 1.2 cm away from the center of the reactor with flowing gases (Fig. S3).

Overall production rates (Fig. 1b, Movies S1 and S2) and the amounts of residual catalysts (Fig. 1c and Fig. S4) and thus the net CNT production rates (Fig. 1d) were significantly affected by the position of the injection tube. As-synthesized CNTs in all cases were highly crystalline ($I_G/I_D > 40$, Fig. 1e and Fig. S5), so they should be dispersible in CSA and spinnable into fiber by wet spinning. The diameters of CNTs ranged from 2 nm to 3 nm (Fig. 1f, Figs. S6 and S7); most were double-walled (Figs. S6 and S8). Considering CNT productivity (~6 mg/min, Fig. 1d) and crystallinity (I_G/I_D ~ 60, Fig. 1e), CNT synthesis was best at position #5 (27 cm and 877 °C) (Movie S2). Most previous studies of CNT synthesis by FCCVD did not consider the depth of injection tube seriously or set the injection tube equivalent to locations #1 to #2 (16 cm and 450 °C) [25,29–32].

Supplementary video related to this article can be found at https://doi.org/10.1016/j.carbon.2020.11.065.

AR is the most important characteristic of CNT for synthesis of CNT-based macrostructures including CNTFs. Direct measurement of ARs of CNTs is only possible for vertically-aligned arrays on a flat substrate. To estimate AR of the dispersed CNTs in CSA, we exploited Onsager theory, which states that the volumetric concentration $\phi_{iso\rightarrow bi}$ [vol%] at which a monodispersed solution of rods undergoes transition from isotropic phase to bi-phase is inversely related to the rods' AR ($\phi_{iso\rightarrow bi}$ [vol%] = $3.34(AR)^{-1}$) [33]. This relationship can also be used to calculate the ARs of CNTs from the measured volumetric transition concentration of CNT solution ($\phi_{iso\rightarrow bi}$ [vol%]) at which CNT solution transits from isotropic (individually dispersed) to bi-phasic (partially LC phase) [34]. The ARs of CNTs determined by observing the isotropic to bi-phasic

based on Onsager theory in the previous study [33,34] and was adopted to estimate the ARs of CNTs synthesized in this work. POM images of CNT solutions with CSA, which were synthesized at the positions of the injection tube (h) #4, (i) #5, and (j) #6, at the lowest concentrations at which bi-phase starts to develop. (A colour version of this figure can be viewed online.)

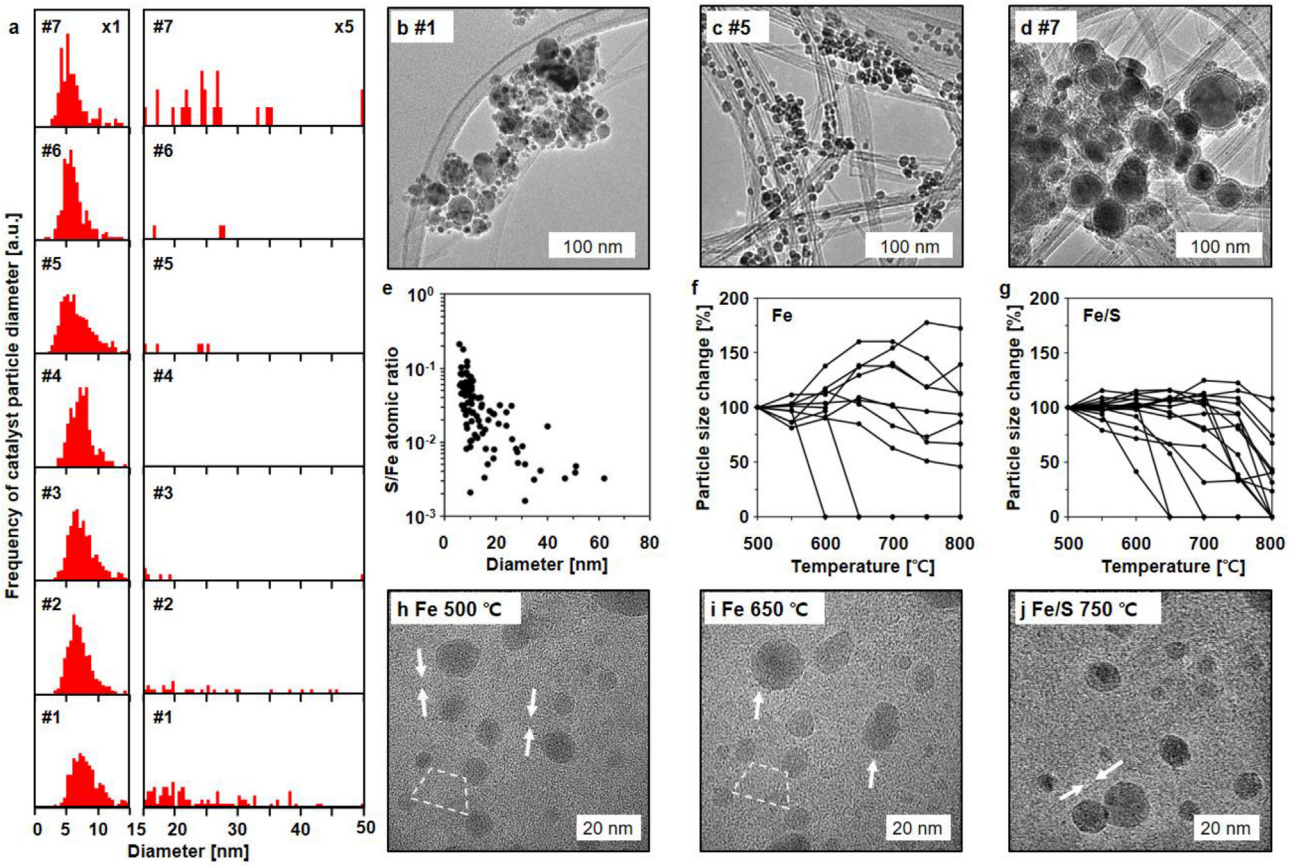

Fig. 2. (*In-situ*) TEM analysis on catalyst particles. (a) Effect of depth of injection tube on change in diameter distributions of catalyst particles. TEM images of catalyst particles in CNTs synthesized at positions (b) #1, (c) #5, and (d) #7. (e) Correlation between sizes and sulfur to iron ratio of the catalyst particles in CNT sample synthesized at position #1. Evolutions in the sizes of (f) iron catalyst particles and (g) iron/sulfur catalyst particles with increasing temperatures from 500 °C to 800 °C (50 °C increments; 5 min hold at each temperature). In-situ TEM images of (h) and (i) iron catalyst particles at 500 °C and 650 °C, and (j) iron/sulfur catalyst particles at 750 °C showing the difference in coalescence behaviors. (A colour version of this figure can be viewed online.)

transition concentration following the Onsager theory were confirmed by cryo-TEM analysis [34]. To measure the ARs of CNTs synthesized at positions #4 (24 cm and 789 °C), #5, and #6 (30 cm and 967 °C), each lowest concentration [mg/mL] at which the bi-phase started to develop was determined by the visible texture in POM images (Fig. 1h–j). Then, each $\phi_{iso\rightarrow bi}$ [mg/mL] was estimated as the average of the highest concentration at which the isotropic phase still exists and the lowest concentration that yielded the bi-phase condition. The volume of CNTs in the solution was calculated from the theoretical density of individual CNT from measured diameters and numbers of walls (Fig. 1f, Figs. S8 and S9) [35] and $\phi_{iso\rightarrow bi}$ [mg/mL] transformed to $\phi_{iso\rightarrow bi}$ [vol%]. Finally, each AR was estimated from the measured $\phi_{iso\rightarrow bi}$ [vol%] value using the developed relationship between AR and $\phi_{iso\rightarrow bi}$ [vol%] in the previous study (Fig. 1g) [34]. The ARs of CNTs synthesized at positions #4, #5, and #6 were 9155, 17812, and 5777, respectively (Fig. 1h–j). The AR of 17812 is by far the highest yet reported among CNTs that can be spun into fiber from LC phase of CNT and CSA solution. Overall, highly-crystalline (I_G/I_D ~ 60, Fig. 1e) CNT with the highest AR (~17812, Fig. 1g and i) were successfully synthesized at high production rate (~6 mg/min, Fig. 1d) by optimizing the depth of the injection tube.

CNT synthesis is correlated with the size distributions of catalyst particles, so we measured them from all samples. The size distributions of the catalyst particles were affected by the depth of the injection tube (Fig. 2a). When CNT synthesis was performed at position #1 of the injection tube, most of the catalyst particles had sizes 5 nm $\leq$ d $\leq$ 15 nm, but a large portion had sizes d > 15 nm (Fig. 2a and b). When CNT synthesis was performed at position #2, the portion of particles that had sizes d > 15 nm was reduced, but some remained. When CNT synthesis was performed at positions #3 (20 cm and 615 °C) to #6 (30 cm and 967 °C), the portion of particles that had sizes d > 15 nm almost vanished and the size distributions of catalyst particles were unimodal with average size d ~ 6 nm (Fig. 2a and c), which is highly preferred for the synthesis of CNTs. However, when the CNT synthesis was conducted at position #7, the portion of particles with sizes d > 15 nm increased again (Fig. 2a and d). Catalyst particles that have sizes d > 15 nm are not expected to grow highly-crystalline CNTs, so this analysis on sizes of catalyst particles explains why the productivity of CNTs was low at positions #1, #2, and #7. Even though the CNTs are not synthesized from all catalyst particles with appropriate sizes, it is clear that the catalyst particles with proper sizes for CNT synthesis are readily formed at positions #4, #5, and #6.

The compositions of catalyst particles from the sample synthesized at position #1 were analyzed using EDS attached to TEM (Fig. 2e). The amount of sulfur increased as the sizes decreased (Fig. 2e and Fig. S10). This result suggests that the iron particles that collide with sulfur early coarsen slowly, whereas those that do not collide early coarsen rapidly until eventually they do collide with sulfur.

Since the formation of the catalyst particles with appropriate sizes before interacting with carbon species is of critical significance to nucleating highly crystalline and high aspect ratio CNTs,

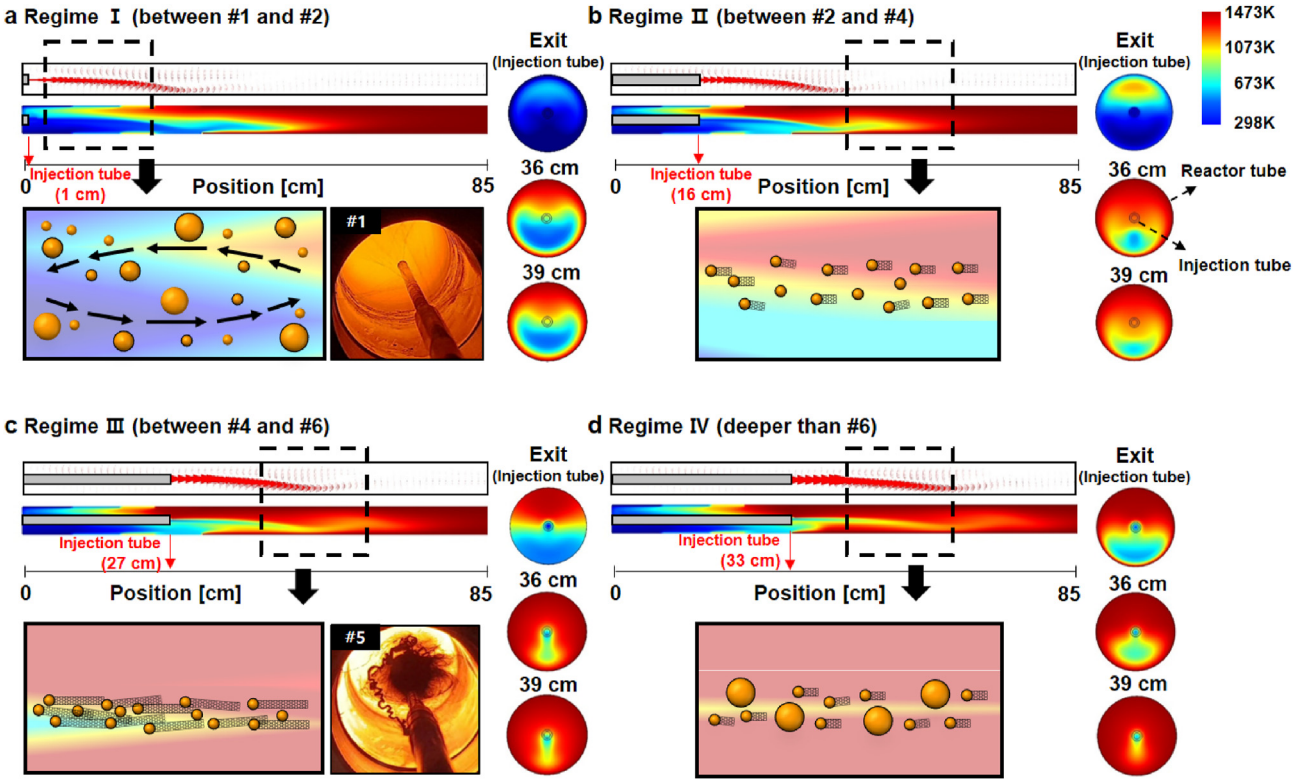

Fig. 3. Fluid dynamics simulation at four injection depths. Longitudinal gas flow patterns and temperature profiles, transverse temperature profiles at each injection tube exit, and 36 cm and 39 cm from the inlet flange of the reactor, and schematic diagrams showing formation of catalyst particles and synthesis of CNTs at injection depths of (a) 1 cm, (b) 16 cm, (c) 27 cm, and (d) 33 cm. Simulation results using injection tubes at different locations (20 cm, 24 cm, 30 cm) are shown in Fig. S13. Digital images in (a) and (c), taken downstream of the reactor, show collection of CNTs. These clearly represent the difference in CNT productivity when CNTs were synthesized at injection positions of #1 and #5, respectively. The simulation was conducted at reactor temperature 1200 °C and total flow rate 3200 sccm ($[H_2]/[Ar] = 0.64$). (A colour version of this figure can be viewed online.)

the effect of sulfur on the evolution of catalyst particle sizes during heating was investigated using in-situ TEM (Fig. 2f–j, Fig. S11, Movies S3 and S4). The iron catalyst particles and iron/sulfur catalyst particles (Fe/S atomic ratio: 10–100) (Fig. S12) were prepared on membrane chips for in-situ heating (Experimental section). Initially the catalyst particles had the size d ~10 nm; the evolution of the size was tracked during in-situ heating from 500 °C to 800 °C (Fig. 2f–g, Fig. S11, Movies S3 and S4). The temperatures were increased in increments of 50 °C at a time and held at each for 5 min.

Supplementary video related to this article can be found at https://doi.org/10.1016/j.carbon.2020.11.065.

Temperature affected the evolution of catalyst particle sizes differently depending on the compositions of the particles. Among iron catalyst particles, some grew (almost doubled), while others shrank, and some even disappeared (Fig. 2f). This phenomenon corresponds to conventional Ostwald ripening [36]. At temperatures ≤650C, iron catalyst particles frequently coalesced (Fig. 2h and i, and Movie S3). In contrast, the sizes of iron/sulfur catalyst particles were generally maintained, but slowly decreased as temperature was increased; this decrease is attributed to evaporation under the high vacuum inside the TEM, rather than to Ostwald ripening. Iron/sulfur catalyst particles did not coalesce well, even when they contacted each other (Fig. 2j and Movie S4). These results indicate that sulfur prevents catalyst particles from becoming too coarsened to actively synthesize high-crystalline CNTs.

The analysis of CNTs (Fig. 1) and catalyst particles (Fig. 2) suggests that the synthesis of CNT by FCCVD can be divided into four regimes depending on the depths of injection tube. Regime I corresponds to the position between injection locations #1 and #2; the catalyst particles have a wide size distribution (i.e., low proportion of optimal sizes), so productivity of CNT is very low. Regime II corresponds to the position between injection locations #2 and #4; the catalyst particles have relatively narrow size distribution around the optimal, and the productivity and AR of CNT increases (but not to the highest). Regime III corresponds to the position between injection locations #4 and #6; the catalyst particles still have narrow size distribution, and the productivity and AR of CNT is among the highest. Regime IV corresponds to positions deeper than #6; the size distribution increases again, and the productivity and AR of CNT decrease.

To understand the why the depth of injection tube affects CNT synthesis, a fluid dynamics simulation was conducted to calculate the gas flow patterns, the temperature profiles inside the reactor and the temperatures at the end of injection tube at each injection depth (Fig. 3, Figs. S13 and S14). In regime I, a vortex is generated ahead of hot reaction zone of the reactor due to the natural convection as the cold reactants are injected into the reactor (Fig. 3a). Therefore, the reactants injected into the reactor are expected to stay ahead of the reaction zone of the reactor for relatively long time and to experience the wide range of temperature variation induced by the convectional vortex. Ferrocene and thiophene have different densities (molar mass), so the long residence time before thermal decomposition in the reaction zone impedes their mixing, so the catalyst particles that form have non-uniform sizes. Synthesis of CNTs from non-uniform sized catalysts leads to very low productivity (digital image in Fig. 3a, and Movie S1).

In regime II, most of the reactants are directly injected into the hot uniform zone of the reactor even though a small vortex is

present (Fig. 3b). In this regime, the effect of the vortex is not significant and large quantities of injected reactants are not expected to stay long ahead of the reaction zone. This good mixing results in the formation of uniform-sized catalyst particles. However, reactants that are not heated enough significantly disturb the temperature profile in the uniform zone of the reactor and this disruption is likely to preclude synthesis of CNTs with high productivity and AR.

In regime III, the reactants are heated enough before they exit the injection tube, so the temperature profile of the reactor is not severely disturbed (Fig. 3c). When the injection tube is located at position #5, the simulation indicates that the temperature at the exit of the injection tube ranges from 260 °C to 510 °C (Fig. S14). Thermal decomposition of ferrocene and thiophene begins at ~400 °C and ~800 °C, respectively [37,38], so most of the ferrocene and thiophene molecules are expected to decompose soon after they exit the injection tube, so the resulting catalyst particles are expected to be of uniform size. Even though the temperature at the inner surface of the injection tube is higher than the decomposition temperature of ferrocene (~510 °C), thin injection tube was not clogged by agglomerated catalyst particles because total flow rate is quite high and thus the residence time of ferrocene inside thin injection tube is very short. The temperature profile of the reaction zone in the reactor is well maintained, so the catalyst particles can effectively produce CNTs with high AR. Since most of reactants are rapidly injected into the reaction zone, thick CNT filament structures are mainly formed, but thin CNT aerogels also coexist (digital image in Fig. 3c, and Movie S2).

In regime IV, the number of ferrocene molecules that start to decompose inside the thin injection tube increases, so large catalyst particles form (Fig. 3d). When the injection tube is located at position #7, the simulation indicates that the temperature at the exit of the injection tube ranges from 350 °C to 630 °C (Fig. S14). Thus, increasing numbers of ferrocene molecules would experience a temperature higher than their thermal decomposition temperature while still inside the injection tube. Increased numbers of collisions among iron atoms released from ferrocene inside the injection tube without sulfur released from thiophene results in rapid formation of large catalyst particles, which reduce the productivity of CNT synthesis (Fig. 3d).

CNT synthesized at position #5 have high crystallinity ($I_G/I_D > 60$), which can facilitate protonation from CSA, so electrostatic repulsion is sufficient to drive spontaneous de-bundling among CNTs, and thus the concentration of CNT in CSA can easily be increased without precipitation. CNT solution with a concentration at 5 mg/mL formed single and full nematic phase without phase separation (Fig. 4a); the POM image clearly shows the disclinations of various signs and strength, which is a typical symbol of Schlieren texture [39], and is similar to that of thermotropic nematic LCs. The birefringent optical texture indicates the local orientation of dispersed CNTs in CSA medium. The birefringent texture (Fig. 4a) exhibits high density of ±1/2 disclinations where a pair of dark brushes that represents CNTs parallel to one of the crossed polarizers meet (Fig. S15) [40,41]. The ±1 disclinations where four dark brushes meet were also observed. The disclination morphology fluctuated during rotation of the sample under crossed polarizers

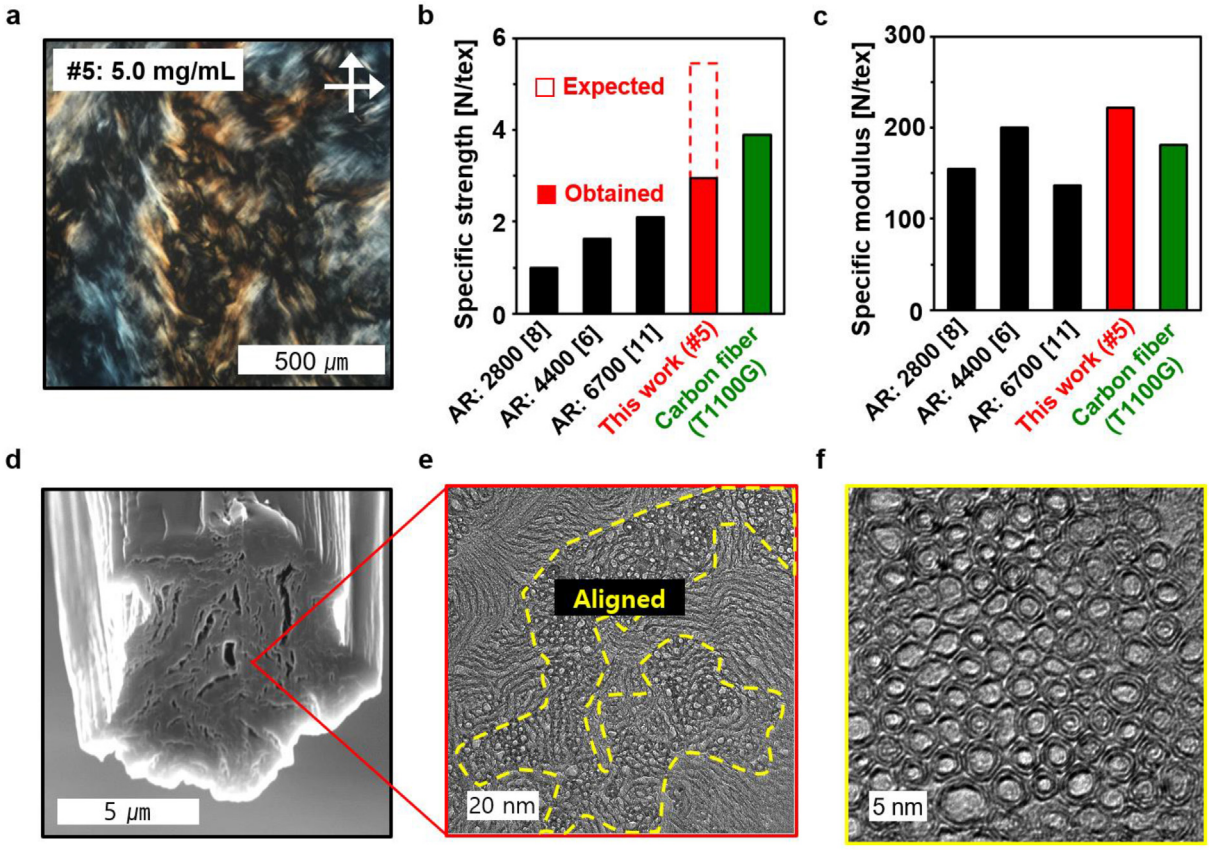

Fig. 4. Fabrication of CNTFs from CNT synthesized at injection point #5. (a) POM image of CNT solution with 5 mg/mL CSA. Comparison of (b) Specific tensile strength and (c) specific tensile modulus of CNTF fabricated in this study with CNTFs from the previous studies [34] and the state-of-the- art carbon fiber (Toray T1100G) (Datasheet of T1100G carbon fiber (Toray)). (d) Cross-sectional SEM image of CNTF showing numbers of voids, (e) cross-sectional TEM image of CNTF that shows aligned and misaligned CNTs along the fiber axis, and (f) magnified TEM image of aligned CNTs that clearly shows their walls. (A colour version of this figure can be viewed online.)

(Movie S5); this phenomenon is usually caused by orientation of well-dispersed CNTs. The features in the POM image indicates unambiguously that the LC phase developed from the CNT synthesized at #5 shows nearly ideal long-range order of CNTs with short-range repulsion mostly owing to CNT characteristics of high crystallinity and high AR.

Supplementary video related to this article can be found at https://doi.org/10.1016/j.carbon.2020.11.065.

A relatively low concentration of CNT solution with the full nematic phase (5 mg/mL) was used for the wet-spinning (Experimental section), because high AR (~17812) of the CNT synthesized at #5 resulted in high enough viscosity for wet spinning even at this low concentration. Our previous study used CNT solution concentration of 20 mg/mL [9]. By exploiting the LC characteristics, the entropy-driven alignment by shearing force in a spinneret is expected to lead to a densified and aligned structure of CNTFs.

As-spun CNTF possessed had the specific tensile strength of 2.94 N/tex and specific tensile modulus of 231 N/tex (Fig. 4b and c, and Fig. S16). This specific strength is the highest reported to date among wet-spun CNTFs, and is comparable to that of the state-of-the-art carbon fiber (Toray T1100G, Fig. 4b). The specific modulus is also the highest among wet-spun CNTFs reported to date and higher than that of the state-of-the-art carbon fiber (Fig. 4c). Assuming the established linear relationship between AR of CNT and the strength of CNTF [6] in the previous study, a CNTF fabricated from CNTs with AR = 17812 is expected to possess the specific strength reaching 6 N/tex, which is much higher than that of the state-of-the-art carbon fiber and our experimental measurements. The lower-than-expected specific strength is attributed to imperfect assembly of CNTs during wet-spinning (Fig. 4d–f). A cross-sectional SEM image of a CNTF shows numbers of large voids (Fig. 4d). The volumetric density of the CNTF is 1.19 g/cm^3 (the linear density/the cross-sectional area), which is lower value than the theoretical density (1.33 g/cm^3). The theoretical density was simply calculated based on the assumption that the CNTF consists of double-walled CNTs with 2.9 nm diameter (Fig. 1f and Fig. S8) and CNTs are hexagonally packed. The presence of such voids in the CNTF deceases the efficiency of load transfer between CNT bundles, so cracks can propagate easily under the tension. Close inspection of the highly densified cress-sectional area of CNTF by TEM shows combined cross-sectional areas composed of randomly misaligned CNTs and aligned CNTs parallel to the axis of CNTF (Fig. 4e). A magnified TEM image (Fig. 4f) of the aligned area of CNTs shows that each strand of CNT is assembled with highly-aligned orientation to the axis of the fiber; this is regarded as an ideal form of CNTF structure. Therefore, if we can use CNTs with AR = 17812 to fabricate a CNTF that consist of only axially-aligned CNTs (Fig. 4f) without any void, it may have specific strength of ~6 N/tex. Therefore, the wet spinning process should be more optimized for high-AR CNTs.

4. Conclusion

The DI-FCCVD method was newly developed to synthesize CNT with high AR (~17812) and high crystallinity (I_G/I_D > 60) by controlling the depth of a thin injection tube into the main horizontal reactor. This method continuously synthesized CNT at relatively high rate (~6 mg/min), so it is expected to be easily scalable to mass production. By deeply inserting thin injection tube into the reactor, the catalyst precursors (ferrocene and thiophene) were well mixed inside the thin tube, and as soon as they left the injection tube, they thermally decomposed and formed catalyst particles with narrow size distribution. Also, the reactants were heated enough inside the thin tube that their injection into the reactor did not disturb the temperature profile in the reaction zone. The CNTF spun from the resulting CNTs had a specific strength of 2.94 N/tex and a specific modulus of 231 N/tex, which are the highest among the wet-spun CNTFs and comparable to those of state-of-the-art carbon fiber. However, the strength of CNTF can still be increased, possibly by optimizing the wet spinning process for high-AR CNTs.

Author contributions

S.-H.L., J.P., J.H.P., D.-M.L., A.L., H.S.J., and S.M.K. conceived and designed the experiments. S.-H.L. and J.H.P. synthesized CNTs using the DI-FCCVD technique. D.-M.L. and H.S.J. performed the experiments to measure the ARs of CNT and of CNTFs fabricated by wet spinning. J.P. and S.Y.M performed the analysis on the catalyst particles and the characteristics of CNTFs. S.Y.L performed the fluid dynamics simulation. S.-H.L., J.P., and S.M.K. wrote the manuscript. S.M.K. supervised the project. All authors discussed the results and contributed to preparation of the manuscript.

Data and materials availability

All data supporting this study and its findings are available within the manuscript and its Supporting Information. Any source data deemed relevant are available from the corresponding author upon request.

CRediT authorship contribution statement

Sung-Hyun Lee: Methodology, Investigation, Formal analysis, Visualization, Writing - original draft. **Junbeom Park:** Methodology, Investigation, Formal analysis, Visualization, Writing - original draft. **Ji Hong Park:** Methodology, Investigation, Formal analysis, Visualization. **Dong-Myeong Lee:** Methodology, Investigation, Formal analysis, Visualization. **Anna Lee:** Methodology, Investigation, Formal analysis. **Sook Young Moon:** Methodology, Investigation, Formal analysis. **Sei Young Lee:** Methodology, Investigation, Formal analysis, Visualization, Writing - review & editing. **Hyeon Su Jeong:** Supervision, Project administration, Writing - review & editing. **Seung Min Kim:** Project administration, Supervision, Conceptualization, Writing - review & editing, Funding acquisition.

Declaration of competing interest

The authors declare that they have no known competing financial interests or personal relationships that could have appeared to influence the work reported in this paper.

Acknowledgments

This work was supported by Samsung Research Funding & Incubation Center of Samsung Electronics under Project Number SRFC-MA1801-06.

Appendix A. Supplementary data

Supplementary data to this article can be found online at https://doi.org/10.1016/j.carbon.2020.11.065.

References

[1] R.H. Baughman, A.A. Zakhidov, W.A. Heer, Carbon nanotubes-the route toward applications, Science 10 (2002) 787.
[2] M.-F. Yu, O. Lourie, M.J. Dyer, K. Moloni, T.F. Kelly, R.S. Ruoff, Strength and breaking mechanism of multiwalled carbon nanotubes under tensile load, Science 287 (2000) 637.
[3] B. Peng, M. Locascio, P. Zapol, S. Li, S.L. Mielke, G.C. Schatz, et al.,

Measurements of near-ultimate strength for multiwalled carbon nanotubes and irradiation-induced crosslinking improvements, Nat. Nanotechnol. 3 (2008) 626.
[4] T.W. Ebbesen, H.J. Lezec, H. Hiura, J.W. Bennett, H.F. Ghaemi, T. Thio, Electrical conductivity of individual carbon nanotubes, Nature 382 (1996) 54.
[5] P. Kim, L. Shi, A. Majumdar, P.L. McEuen, Thermal transport measurements of individual multiwalled nanotubes, Phys. Rev. Lett. 87 (2001) 215502.
[6] D.E. Tsentalovich, R.J. Headrick, F. Mirri, J. Hao, N. Behabtu, C.C. Young, et al., Influence of carbon nanotube characteristics on macroscopic fiber properties, ACS Appl. Mater. Interfaces 9 (2017) 36189.
[7] L.M. Ericson, H. Fan, H. Peng, V.A. Davis, W. Zhou, J. Sulpizio, et al., Macroscopic, neat, single-walled carbon nanotube fibers, Science 305 (2004) 1447.
[8] N. Behabtu, C.C. Young, D.E. Tsentalovich, O. Kleinerman, X. Wang, A.W.K. Ma, et al., Strong, light, multifunctional fibers of carbon nanotubes with ultrahigh conductivity, Science 339 (2013) 182.
[9] J. Lee, D.M. Lee, Y.K. Kim, H.S. Jeong, S.M. Kim, Significantly increased solubility of carbon nanotubes in superacid by oxidation and their assembly into high-performance fibers, Small 13 (2017) 1701131.
[10] A.R. Bucossi, C.D. Cress, C.M. Schauerman, J.E. Rossi, I. Puchades, B.J. Landi, Enhanced electrical conductivity in extruded single-wall carbon nanotube wires from modified coagulation parameters and mechanical processing, ACS Appl. Mater. Interfaces 7 (2015) 27299.
[11] L.W. Taylor, O.S. Dewey, R.J. Headrick, N. Komatsu, N.M. Peraca, G. Wehmeyer, et al., Improved properties, increased production, and the path to broad adoption of carbon nanotube fibers, Carbon 171 (2021) 689–694.
[12] V.A. Davis, A.N.G. Parra-Vasquez, M.J. Green, P.K. Rai, N. Behabtu, V. Prieto, et al., True solutions of single-walled carbon nanotubes for assembly into macroscopic materials, Nat. Nanotechnol. 4 (2009) 830.
[13] A.N.G. Parra-Vasquez, N. Behabtu, M.J. Green, C.L. Pint, C.C. Young, J. Schmidt, et al., Spontaneous dissolution of ultralong single- and multiwalled carbon nanotubes, ACS Nano 4 (2010) 3969.
[14] M.S. Motta, A. Moisala, I.A. Kinloch, A.H. Windle, The role of sulphur in the synthesis of carbon nanotubes by chemical vapour deposition at high temperatures, J. Nanosci. Nanotechnol. 8 (2008) 2442–2449.
[15] S.M. Kim, C.L. Pint, P.B. Amama, D.N. Zakharov, R.H. Hauge, B. Maruyama, et al., Evolution in catalyst morphology leads to carbon nanotube growth termination, J. Phys. Chem. Lett. 1 (2010) 918.
[16] C.-H. Lee, J. Lee, J. park, E. Lee, S.M. Kim, K.H. Lee, Rationally designed catalyst layers toward “immortal” growth of carbon nanotube forests: Fe-ion implanted substrates, Carbon 152 (2019) 482.
[17] Q. Zhang, J.-Q. Huang, M.-Q. Zhao, W.-Z. Qian, F. Wei, Modulating the diameter of carbon nanotubes in array form via floating catalyst chemical vapor deposition, Appl. Phys. A 94 (2009) 853–860.
[18] M. Fulem, K. Ruzicka, M. Ruzicka, Recommended vapor pressures for thiophene, sulfolane, and dimethyl sulfoxide, Fluid Phase Equil. 303 (2011) 205–216.
[19] S.-H. Lee, J. Park, H.-R. Kim, T. Lee, J. Lee, Y.-O. Im, et al., Synthesis of carbon nanotube fibers using the direct spinning process based on design of experiment (DOE), Carbon 100 (2016) 647.
[20] Y.L. Li, I.A. Kinloch, A.H. Windle, Direct spinning of carbon nanotube fibers from chemical vapor deposition synthesis, Science 302 (2004) 276.
[21] M.S. Motta, A. Moisala, I.A. Kinloch, A.H. Windle, The role of sulphur in the synthesis of carbon nanotubes by chemical vapour deposition at high temperatures, J. Nanosci. Nanotechnol. 8 (2008) 2442.
[22] V. Reguero, B. Alemán, B. Mas, J.J. Vilatela, Controlling carbon nanotube type in macroscopic fibers synthesized by the direct spinning process, Chem. Mater. 26 (2014) 3550.
[23] J. Lee, D.M. Lee, Y. Jung, J. Park, H.S. Lee, Y.K. Kim, et al., Direct spinning and densification method for high-performance carbon nanotube fibers, Nat. Commun. 10 (2019) 2962.
[24] Y. Jung, J. Song, W. Huh, D. Cho, Y. Jeong, Controlling the crystalline quality of carbon nanotubes with processing parameters from chemical vapor deposition synthesis, Chem. Eng. J. 228 (2013) 1050.
[25] C. Paukner, K.K. Koziol, Ultra-pure single wall carbon nanotube fibres continuously spun without promoter, Sci. Rep. 4 (2014) 3903.
[26] S.-H. Lee, H.R. Kim, T. Lee, H. Lee, J. Lee, J. Lee, et al., Synthesis of carbon nanotube fibers from carbon precursors with low decomposition temperatures using a direct spinning process, Carbon 124 (2017) 219.
[27] L. Weller, F.R. Smail, J.A. Elliott, A.H. Windle, A.M. Boies, S. Hochgreb, Mapping the parameter space for direct-spun carbon nanotube aerogels, Carbon 146 (2019) 789.
[28] C.J. An, Y.H. Kang, A.Y. Lee, K.S. Jang, Y. Jeong, S.Y. Cho, Foldable thermoelectric materials: improvement of the thermoelectric performance of directly spun CNT webs by individual control of electrical and thermal conductivity, ACS Appl. Mater. Interfaces 8 (2016) 22142.
[29] J.N. Wang, X.G. Luo, T. Wu, Y. Chen, High-strength carbon nanotube fibre-like ribbon with high ductility and high electrical conductivity, Nat. Commun. 5 (2014) 3848.
[30] T.S. Gspann, F.R. Smail, A.H. Windle, Spinning of carbon nanotube fibres using the floating catalyst high temperature route: purity issues and the critical role of sulphur, Faraday Discuss 173 (2014) 47.
[31] W. Xu, Y. Chen, H. Zhan, J.N. Wang, High-strength carbon nanotube film from improving alignment and densification, Nano Lett. 16 (2016) 946.
[32] B. Aleman, V. Reguero, B. Mas, J.J. Vilatela, Strong carbon nanotube fibers by drawing inspiration from polymer fiber spinning, ACS Nano 9 (2015) 7392–7398.
[33] L. Onsager, Ann. N.Y. The effects of shape on the interaction of colloidal particles, Acd. Sci. 51 (1949) 627.
[34] D.E. Tsentalovich, A.W.K. Ma, J.A. Lee, N. Behabtu, E.A. Bengio, A. Choi, et al., Relationship of extensional viscosity and liquid crystalline transition to length distribution in carbon nanotube solutions, Macromolecules 49 (2016) 681.
[35] C. Laurent, E. Flahaut, A. Peigney, The weight and density of carbon nanotubes versus the number of walls and diameter, Carbon 48 (2010) 2994.
[36] I.M. Lifshitz, V.V. Slyozov, The kinetics of precipitation from supersaturated solid solutions, J. Phys. Chem. Solid. 19 (1961) 35.
[37] R.M. Sundaram, K.K. Koziol, A.H. Windle, Continuous direct spinning of fibers of single-walled carbon nanotubes with metallic chirality, Adv. Mater. 23 (2011) 5064.
[38] S.-H. Lee, J. Park, H.-R. Kim, J. Lee, K.-H. Lee, Synthesis of high-quality carbon nanotube fibers by controlling the effects of sulfur on the catalyst agglomeration during the direct spinning process, RSC Adv. 5 (2015) 41894.
[39] W. Song, I.A. Kinloch, A.H. Windle, Nematic liquid crystallinity of multiwall carbon nanotubes, Science 302 (2003) 1363.
[40] W. Song, A.H. Windle, Isotropic-nematic phase transition of dispersions of multiwall carbon nanotubes, Macromolecules 38 (2005) 6181.
[41] J.-Y. Song, H.-J. Kang, J.C. Won, Y.H. Kim, Y.-S. J, H.S. Jeong, The true liquid crystal phases of 2D polymeric carbon nitride and macroscopic assembled fibers, Mater. Horiz. 6 (2019) 1726.